ACS APPLIED MATERIALS & INTERFACES

Research Article

Cite This: ACS Appl. Mater. Interfaces 2018, 10, 1399−1407

www.acsami.org

Nickel Nanoparticle Encapsulated in Few-Layer Nitrogen-Doped Graphene Supported by Nitrogen-Doped Graphite Sheets as a High-Performance Electromagnetic Wave Absorbing Material

Haoran Yuan,[†,‡,§] Feng Yan,[†] Chunyan Li,[†] Chunling Zhu,[*,‡] Xitian Zhang,[§] and Yujin Chen[*,†]

[†]Key Laboratory of In-Fiber Integrated Optics, Ministry of Education, and College of Science, and [‡]College of Material Science and Chemical Engineering, Harbin Engineering University, Harbin 150001, China

[§]Key Laboratory for Photonic and Electronic Bandgap Materials, Ministry of Education, and School of Physics and Electronic Engineering, Harbin Normal University, Harbin 150025, China

Supporting Information

ABSTRACT: Herein we develop a facile strategy for fabricating nickel particle encapsulated in few-layer nitrogen-doped graphene supported by graphite carbon sheets as a high-performance electromagnetic wave (EMW) absorbing material. The obtained material exhibits sheetlike morphology with a lateral length ranging from a hundred nanometers to 2 μm and a thickness of about 23 nm. Nickel nanoparticles with a diameter of approximately 20 nm were encapsulated in about six layers of nitrogen-doped graphene. As applied for electromagnetic absorbing material, the heteronanostructures exhibit excellent electromagnetic wave absorption property, comparable to most EMW absorbing materials previously reported. Typically, the effective absorption bandwidth (the frequency region falls within the reflection loss below −10 dB) is up to 8.5 GHz at the thicknesses of 3.0 mm for the heteronanostructures with the optimized Ni content. Furthermore, two processes, carbonization at a high temperature and subsequent treatment in hot acid solution, were involved in the preparation of the heteronanostructures, and thus, mass production was achieved easily, facilitating their practical applications.

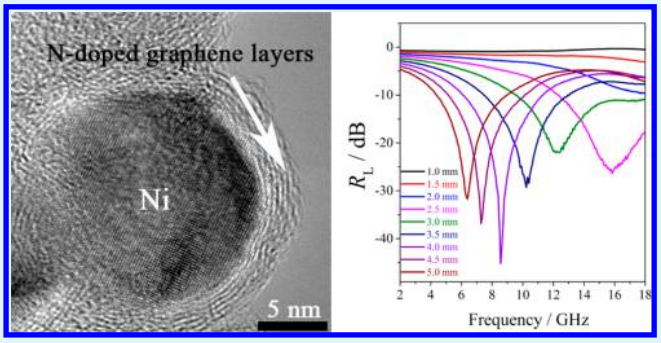

KEYWORDS: *nickel nanoparticles, N-doped graphene, heteronanostructures, electromagnetic wave, absorption property*

1. INTRODUCTION

Electromagnetic wave (EMW) absorbing materials have attracted increasing attention due to increasing EM interference problems induced by wide utilization of electronic devices operating at the gigahertz band. To date, EMW absorbing materials have been required to possess advantages such as being light and thin and having wide absorption band, strong absorption performance, high stability, and antioxidation properties. Soft magnetic metals have potential applications in the EMW absorption field due to their high Snoek limit.[1] However, the EMW absorption properties of soft magnetic metals are limited by their serious aggregation phenomena and poor antioxidation. Therefore, several special structures including core−shelled, yolk−shelled, and encapsulated materials containing soft magnetic metals have been developed to overcome those drawbacks of the soft magnetic metals.[2−18] Among these materials, core−shelled or encapsulated structures have exhibited attractive EMW absorption performance.[2−8] For example, the reflection loss (R_L) Ni−Ag core−shelled nanoparticles was −23.6 dB at an optimal frequency of 10.8 GHz.[2] Ni/C nanocapsules exhibited comparable EMW absorption property with a maximum R_L value of −40 dB at 3 GHz.[4] The large absorption bandwidth below −10 dB was achieved by ZnO-coated Ni nanoparticles.[6] However, some drawbacks need to be further solved for their practical applications: (i) the addition amount of those structures into the matrixes such as paraffin was larger than 40 wt %; (ii) even encapsulated in foreign materials, the aggregations between the magnetic metals were still observed;[2−8] (iii) some outmost coatings such as ZnO may not impede the oxidation of the inner magnetic metal core efficiently upon air exposure for long time; (iv) most of those materials were prepared by an arc-discharge technique, and mass-production was achieved difficultly.

Recently, ultrathin two-dimensional materials such as graphene have attracted much attention due to their excellent physicochemical properties. As for applications in the EMW absorption field, graphene sheets were commonly used as substrates for supporting nanostructures.[19−39] By reasonable structure designation, those graphene-based composites showed enhanced EMW absorption properties in comparison to single counterparts.[19−39] Especially, coupling the magnetic nanomaterials with graphene sheets could efficiently improve

Received: October 14, 2017
Accepted: December 7, 2017
Published: December 7, 2017

DOI: 10.1021/acsami.7b15559
ACS Appl. Mater. Interfaces 2018, 10, 1399−1407

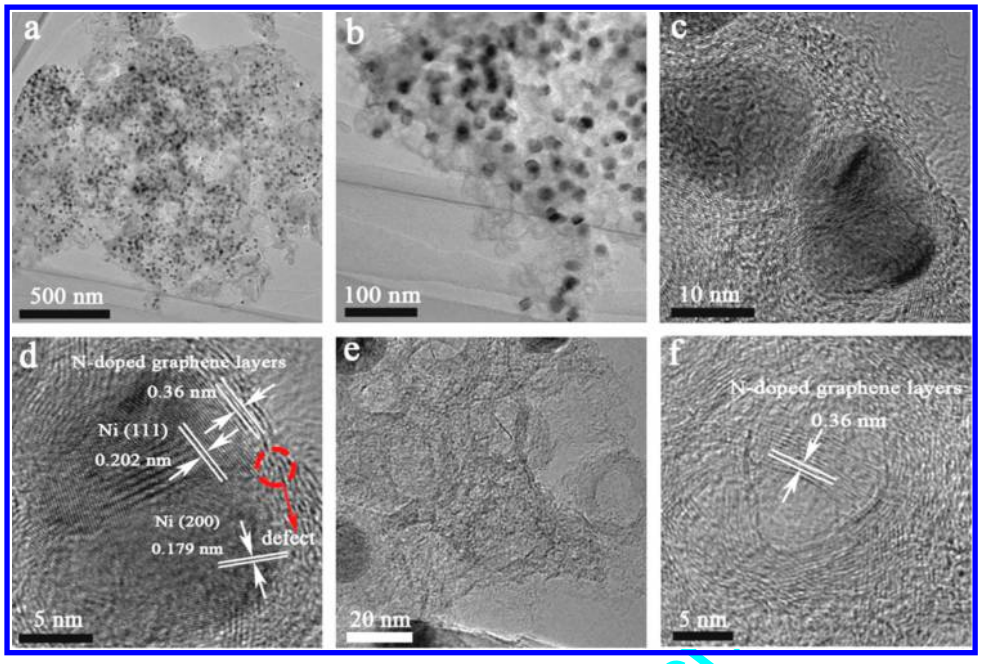

Figure 1. TEM images of the Ni@NG/NC nanosheets: (a and b) low-magnification and high-magnification TEM images for individual Ni@NG/NC nanosheets; (c and d) HRTEM images for Ni NPs encapsulated in few-layer N-doped graphene; (e and f) low-magnification and HRTEM images for onion-like carbon nanostructures.

EMW absorption properties.[23−39] For example, Pan et al. prepared Co/G composites through a phase-controlled strategy and found that the α-Co/G composite exhibited enhanced EMW absorption property with a minimal R_L value of −47.5 dB at 11.9 GHz.[32] Our previous result showed that coupling hollow Fe_3O_4−Fe nanoparticles with graphene could improve the EMW absorption property of the composite.[34] Qi et al. designed a heteronanostructure that consisted of metal cobalt, carbon nanotube, and graphene with an optimal R_L value of −65.5 dB at 12.4 GHz.[39] On the basis of the above results, it can be concluded that construction of magnetic graphene-based composites is an efficient way for development of high-performance EMW absorbing materials.

Nitrogen-doped carbonaceous materials have been reported to show significantly enhanced physicochemical properties and have been widely applied in energy storage and conversion systems. However, the EMW absorption properties of magnetic metal nanoparticles encapsulated in nitrogen-doped graphene have been investigated rarely so far. Herein, we develop a facile method to synthesize nickel nanoparticle encapsulated in few-layer nitrogen-doped graphene supported by nitrogen-doped graphite sheets (Ni@NG/NC). The heteronanostructured Ni@NG/NC used as an EMW absorbing material possesses the following advantages: (i) the Ni nanoparticles (NPs) with a diameter of 20 nm were encapsulated in few-layer nitrogen-doped graphene, leading to their robust stability against strong acidic solution and strong antioxidation upon air exposure; (ii) the graphene-encapsulated Ni NPs were uniformly separated between each other, avoiding the serious aggregation among those magnetic NPs; (iii) the graphene-encapsulated Ni NPs were supported by N-doped graphite nanosheets, endowing numerous interfaces to the heteronanostructures; (iv) two processes, carbonization at a high temperature and subsequent treatment in hot acid solution, were involved in the preparation of the heteronanostructures, and mass-production was achieved easily. As a consequence, even as the addition amount into the paraffin matrix was only 20 wt %, Ni@NG/NC exhibited excellent EMW absorption property, comparable to most EMW absorbing materials previously reported.

2. EXPERIMENTAL SECTION

2.1. Preparation of Ni@NG/NC. Urea and nickel acetylacetonate with molar ratio of 6:1 were uniformly mixed, and then the mixture was heated at 900 °C for 1 h under Ar protection. The obtained black powder was treated in 0.5 M H_2SO_4 at 160 °C for 12 h. The final product was washed with water and dried at 40 °C for 24 h under vacuum.

2.2. Characterizations. The structures of the samples were characterized by X-ray powder diffraction (XRD) using an X'Pert Pro diffractometer with Cu Kα radiation (λ = 1.5418 Å), scanning electron microscopy (SEM) using a Hitachi SU8000, and transmission electron microscopy (TEM, JEM-2010, JEOL); X-ray photoelectron spectroscopy (XPS) data were taken on an X-ray photoelectron spectrometer (K-Alpha,Thermofisher Scientific Company) with Al Kα radiation generated at 12 kV and 150 W. The surface areas of samples were tested by nitrogen adsorption/desorption analysis (TRISTAR II3020). Raman spectra were recorded on a Raman spectrometer (Lab RAMA ramis, Horiba Jobin Yvon) using a 488 nm He−Ne laser. The Ni content in Ni@NG/NC was determined by a thermogravimetric analyzer (Diamond TG-DTA). The atomic force image (AFM) was recorded on a scanning probe microscope (CSPM 5500). The magnetic property of the Ni@NG/NC nanosheets was measured by a vibrating sample magnetometer (VSM; Lakeshore 7410) at room temperature.

2.3. Electromagnetic Parameter Measurement. The electromagnetic parameters of the absorbing materials were measured by using a vector network analyzer (Anritsu MS4644A Vectorstar). The cylindrical sample (with 3.00 mm inner diameter, 7.00 mm outer diameter, and 3.00 mm thickness) was prepared by mixing Ni@NG/NC with a paraffin matrix. The addition amount of Ni@NG/NC to paraffin matrix was controlled to be 20 wt %.

3. RESULTS AND DISCUSSION

3.1. Structural Characterization of Ni@NG/NC Nanosheets. Because two processes, carbonization at a high

DOI: 10.1021/acsami.7b15559
ACS Appl. Mater. Interfaces 2018, 10, 1399−1407

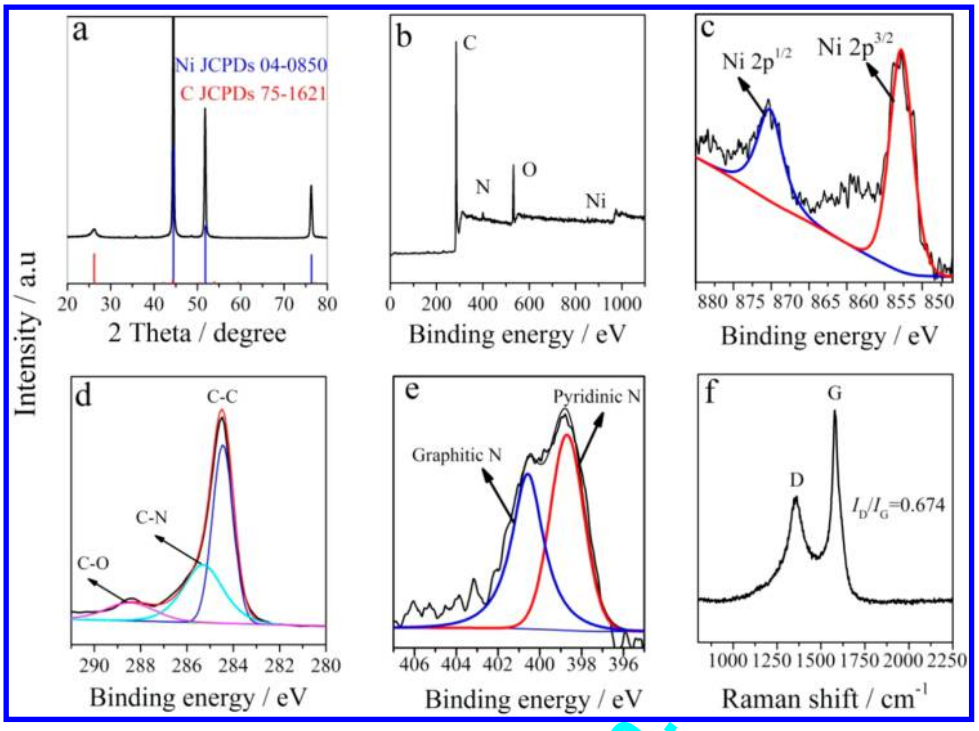

Figure 2. (a) XRD pattern, (b) the survey XPS spectrum, (c) Ni 2p core level XPS spectrum, (d) C 1s core level XPS spectrum, (e) N 1s core level XPS spectrum, and (f) Raman spectrum of the Ni@NG/NC nanosheets.

temperature and subsequent treatment in hot acid solution, were involved in the preparation of the heteronanostructures, several grams of Ni@NG/NC could be produced in one batch. Therefore, the strategy for the synthesis of Ni@NG/NC could be scaled up to industrial production. Figure S1a (Supporting Information) shows a typical SEM image of Ni@NG/NC. It can be found that Ni@NG/NC exhibits sheetlike morphology with lateral length ranging from a hundred nanometers to 2 μm. The AFM image (Figure S1b, Supporting Information) indicates that the thickness of the nanosheets is about 23 nm. A low-magnification TEM image reveals that Ni NPs are uniformly distributed in the Ni@NG/NC nanosheets with a lateral length of around 2 μm (Figure 1a). The uniform distribution of small Ni particles is confirmed by the energy-dispersive X-ray spectrometry (EDX) elemental mapping images of the Ni@NG/NC nanosheets (Figure S2, Supporting Information). Figure 1b indicates that the diameter of the Ni NPs is approximately 20 nm. High-resolution TEM (HRTEM) analysis indicates that the Ni NPs are encapsulated in about six layers of graphene shell (Figure 1, parts c and d). The well-resolved lattice fringes with *d*-spacings of 0.202 and 0.179 nm in the Ni core region can be clearly observed in the HRTEM image, which correspond to the (111) and (200) planes of Ni NPs (Figure 1d). In the graphene shell region, the interlayer distance is around 0.36 nm, confirming that the Ni NPs are coated by the graphene layers (Figure 1d). Selected area electron diffraction (SAED) displays the diffraction rings from the (002) plane of graphite carbon, and (111), (200), and (220) planes of Ni, and further confirms the presence of the graphite carbon and crystal Ni in the Ni@NG/NC nanosheets (Figure S3, Supporting Information). In addition, onion-like nanostructures with an interlayer distance of 0.36 nm can be clearly observed in some regions without Ni NPs, suggesting a porous feature of the Ni@NG/NC nanosheets (Figure 1, parts e and f). The formation of such onion-like nanostructures can be attributed to the removal of the Ni NPs in completely encapsulated within N-doped graphene shells after the nanosheets were treated in the hot acidic solution. The porous feature is further confirmed by nitrogen adsorption−desorption isotherms analysis (Figure S4, Supporting Information). The Ni@NG/NC nanosheets exhibit type IV hysteresis (Figure S4a, Supporting Information), suggesting the presence of mesopores in the nanosheets. The Brunauer−Emmett−Teller (BET) surface area of Ni@NG/NC nanosheets is calculated to be 89.7 $m^2\ g^{-1}$. Using the Barrett−Joyner−Halenda (BJH) method, the average pore size is about 3.8 nm, and the corresponding BJH desorption cumulative pore volume is as 0.116 $cm^3\ g^{-1}$ (Figure S4b, Supporting Information). Notably, if the treatment of the annealed sample in hot acidic solution was left out, besides small Ni NPs, many large Ni particles with a size at a micrometer level were found to be loaded on the obtained nanosheets (Figure S5, Supporting Information). Thus, the treatment in hot acidic solution is a key process for the preparation of the nanosheets with uniform distribution of small Ni NPs. Our previous results showed that the Ni NPs anchored on the graphene sheets were oxidized to form a thin NiO layer even with exposure to air at room temperature, and totally transformed to NiO NPs after heating the composite at 200 °C for 3 h and 280 °C for another 3 h under air atmosphere.[48] In contrast, even after the Ni@NG/NC nanosheets were heated at 300 °C for 12 h under air atmosphere, most of Ni NPs in the nanosheets could not be oxidized to NiO NPs, as evidenced by XRD measurements (Figure S6, Supporting Information). There results above demonstrate that the Ni NPs encapsulated in few-layer nitrogen-doped graphene have strong resistance to hot acidic corrosion and oxidation characters.

Figure 2a shows the XRD pattern of the Ni@NG/NC nanosheets. The diffraction peaks at 2θ 44.5°, 51.8°, and 76.3° can be assigned to the (111), (200), and (220) planes of the Ni

DOI: 10.1021/acsami.7b15559
ACS Appl. Mater. Interfaces 2018, 10, 1399−1407

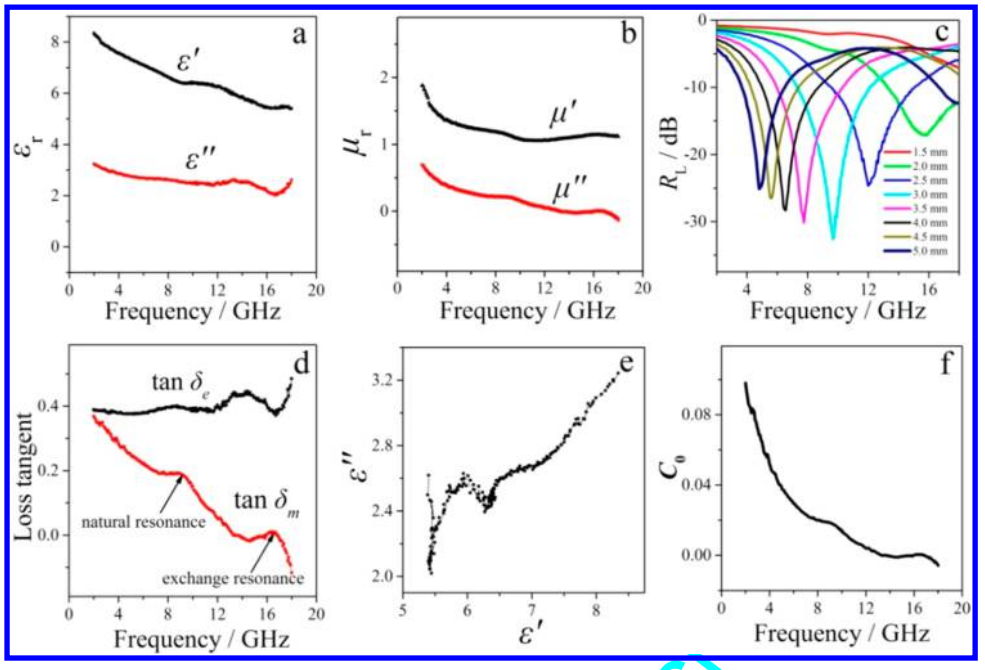

Figure 3. (a) Relative complex permittivity, (b) the relative complex permeability, (c) R_L–f curves, and (d) loss tangent data of the Ni@NG/NC nanosheets. (e and f) Cole–Cole and C_0–f plots for Ni@NG/NC nanosheets.

NPs (JCPDS 04-0850), respectively, where the peak centered at 26.2° corresponds to the (002) plane of graphitic carbon (JCPDS 75-1621).The diffraction peaks from nickel oxides or hydroxides are not detected, suggesting strong antioxidation of the Ni NPs due to the protection of the N-doped graphene shell. The surface composition and chemical valence states of the Ni@NG/NC nanosheets were characterized by XPS analysis. The survey spectrum (Figure 2b) suggests the presence of Ni, C, O, and N elements in the Ni@NG/NC nanosheets. In the Ni 2p XPS spectrum (Figure 2c), the peaks at 852.3 and at 870.0 eV are observed in the Ni $2p_{3/2}$ and Ni $2p_{1/2}$ regions, respectively, which can be assigned to the binding energies of metallic nickel.[40] Obvious peaks corresponding to high oxidation state of nickel are not found, further confirming the excellent antioxidation of the Ni NPs in the Ni@NG/NC nanosheets. The C 1s XPS spectrum (Figure 2d) can be deconvoluted into three peaks at 284.5, 285.8, and 288.5 eV, which correspond to C–C, C–N, and C–O groups, respectively.[41−43] In the N 1s spectrum (Figure 2e), there are two peaks centered at 398.2 and 400.6 eV, corresponding to pyridinic N and graphitic N, respectively.[43] The N content in the Ni@NG/NC nanosheets is estimated to be 2.3 atom % according to the XPS data. The existence of N element is further confirmed by EDX mapping images, as shown in Figure S7 (Supporting Information). TG analysis demonstrates that the Ni content in the Ni@NG/NC nanosheets is about 55 wt % (Figure S8, Supporting Information). Figure 2f displays the Raman spectrum of the Ni@NG/NC nanosheets in the Raman shift ranging from 800 to 2250 cm^{-1}. Two peaks at about 1350 and 1580 cm^{-1} are found for the nanosheets, characteristic feature of carbonaceous materials. The peak at 1350 cm^{-1} (D band) corresponds to the defect in the carbon, whereas the peak at 1580 cm^{-1} (G band) is due to graphitic carbon. The intensity ratio of the D and G bands (I_D/I_G) is about 1:1.5, suggesting a higher degree of graphitization of carbon in the Ni@NG/NC nanosheets, which is consistent with XRD and TEM results.

3.2. Magnetic and EMW Absorption Properties of Ni@NG/NC Nanosheets. The field dependence of magnetization for the Ni@NG/NC nanosheets was measured by a vibrating sample magnetometer at room temperature, as shown in Figure S9 (Supporting Information). Significant hysteresis loops in the M–H curves indicate the ferromagnetic property of the Ni@NG/NC nanosheets. The saturation magnetization (M_s), coercivity (H_c), and retentivity (M_r) for the nanosheets are 23.5 emu/g, 67.1 Oe, and 1.2 emu/g, respectively. The Ni@NG/NC nanosheets show the ferromagnetic behavior, which may facilitate the EMW absorption property.[23−39]

The electromagnetic parameters of the paraffin composite containing 20 wt % of the Ni@NG/NC nanosheets were measured at room temperature to investigate the EMW absorption property of the nanosheets. The electromagnetic parameters include relative complex permittivity, $\varepsilon_r = \varepsilon' - j\varepsilon''$, and the relative complex permeability, $\mu_r = \mu' - j\mu''$. ε_r and μ_r, relevant to dielectric and magnetic losses, respectively, have important effects on the EMW absorption property of absorbing materials. As shown in Figure 3a, both ε' and ε'' gradually decrease with an increase of frequency and are in range of 5.39–5.35 and 2.60–3.25, respectively. The μ' and μ'' are varied in range of 1.08–1.89 and −0.13–1.08, respectively (Figure 3b). The real parts and imaginary parts of the relative complex permeability and relative complex permittivity have relatively large values, implying that the Ni@NG/NC nanosheets have good EMW absorption property. The R_L value can be calculated by the following equations according to transmission line theory:[44]

$$Z_{in} = Z_0(\mu_r/\varepsilon_r)^{1/2} \tanh[j2\pi fd/c(\mu_r\varepsilon_r)^{1/2}] \quad (1)$$

$$R_L\ (\mathrm{dB}) = 20 \log \left| \frac{Z_{in} - Z_0}{Z_{in} + Z_0} \right| \quad (2)$$

where Z_0 is the impedance of free space, Z_{in} is the input impedance of the absorber, c is the velocity of electromagnetic

DOI: 10.1021/acsami.7b15559
ACS Appl. Mater. Interfaces 2018, 10, 1399–1407

waves in free space, f is the frequency of microwaves, and d is the thickness of the absorber. When the R_L value is below −10 dB, more than 90% of EMW energy will be absorbed, which means that the absorber can be applied practically. The corresponding frequency range is defined as effective absorption bandwidth (EAB). As for practical application of the absorbing material, the EAB is required to be as large as possible at a given thickness. Figure 3c shows R_L−f curves of the Ni@NG/NC nanosheets at various thicknesses. At the thicknesses of 2.0, 2.5, 3.0, 4.0, 4.5, and 5.0 mm, all of the minimum R_L ($R_{L,min}$) values are below −10 dB for the Ni@NG/NC nanosheets, and the corresponding EABs are 4.8, 5.2, 4.9, 4.4, 3.7, 3.2, and 2.9 GHz, respectively. The EMW absorption property of the Ni@NG/NC nanosheets is among the best absorption properties of the magnetic materials previously reported, as shown in Table S1 (Supporting Information). Furthermore, the addition amount of the Ni@NG/NC nanosheets is only 20 wt %, which is smaller than those of the magnetic materials previously reported (Table S1, Supporting Information). Therefore, the Ni@NG/NC nanosheets have very promising application in EMW absorption field.

3.3. Mechanism on EMW Absorption Properties of Ni@NG/NC Nanosheets. To uncover the mechanism of the good EMW absorption property of the Ni@NG/NC nanosheets, the dielectric loss tangent ($\tan \delta_e = \varepsilon''/\varepsilon'$) and magnetic loss tangent ($\tan \delta_m = \mu''/\mu'$) were calculated. As shown in Figure 3d, $\tan \delta_e$ is in the range of 0.38−0.49 with a slight fluctuation at the high-frequency region.

The large $\tan \delta_e$ demonstrates that dielectric loss contributes to the EMW absorption property of the Ni@NG/NC nanosheets over the full tested frequency region. As for $\tan \delta_m$, the value falls within the range of 0.15−0.37 at the low-frequency band (2−10 GHz), and then decreases rapidly at the high-frequency region (10−18 GHz). This result suggests that magnetic loss contributes to the EMW absorption property of the Ni@NG/NC nanosheets only at the low-frequency region.

The dielectric loss is closely relevant to the dielectric relaxation processes, which can be explained by the Cole−Cole curves. According to the Debye theory, the relationships between ε'' and ε' can be written as

$$(\varepsilon' - (\varepsilon_s + \varepsilon_\infty)/2)^2 + (\varepsilon'')^2 = ((\varepsilon_s - \varepsilon_\infty)/2)^2 \quad (3)$$

where ε_s and ε_∞ are the static permittivity and the relative dielectric permittivity at high-frequency limit. Figure 3e shows the Cole−Cole curve of the N-doped carbon nanosheets plotted in terms of eq 3. Two clear semicircles are observed in the Cole−Cole curve, suggesting that multirelaxation processes will occur when the electromagnetic wave irradiates the Ni@NG/NC nanosheets. The two dielectric relaxations can be attributed to dipole polarization and interfacial polarization. The dipole polarization is usually produced by defects, dangling bands, or unsaturated coordination in the absorbing materials upon electromagnetic field irradiation. In our Ni@NG/NC nanosheets, there are numerous defects caused by N-doping and non-graphitic carbon, evidenced by HRTEM and Raman measurements (Figure 1d, Figure 2f). In addition, the unsaturated coordination groups such C−O and C−N are presented in the nanosheets (Figure 2, parts d and e). Those defects and unsaturated coordination groups can act as polarized centers, which contribute to the dielectric relaxations of the Ni@NG/NC nanosheets. Furthermore, multi-interfaces, such as the interface between Ni NPs and N-doped graphene and the interface between N-doped graphene and N-doped carbon nanosheets, exist in the Ni@NG/NC nanosheets. The redistribution of the charges at the interfacial regions will occur upon EMW irradiation, and thus, the interfacial polarization contributes to the dielectric relaxations of the Ni@NG/NC nanosheets. As a consequence, the dipole and interfacial polarizations, induced by defects/unsaturated coordination groups and interfaces, respectively, result in large dielectric loss of our Ni@NG/NC nanosheets.

In general, the magnetic loss comes from hysteresis loss, domain-wall resonance, eddy current effect, natural resonance, and exchange resonance. However, the contributions of hysteresis loss and domain-wall resonance to the magnetic loss can be excluded because they common occur merely under strong electromagnetic field irradiation and at a frequency region below 2 GHz for ferromagnetic materials, respectively. The imaginary part of relative complex permeability relevant to the eddy current effect can be described by[45,46]

$$\mu'' = 2\pi\mu_0(\mu')^2\sigma d^2 f/3 \quad (4)$$

where μ_0 and σ are the permeability of vacuum and the electric conductivity, respectively. Defining the constant C_0 equal to $2\pi\mu_0\sigma d^2/3$, the following equation will be obtained:

$$C_0 = 2\pi\mu_0\sigma d^2/3 = \mu''(\mu')^{-2}f^{-1} \quad (5)$$

In terms of the eq 5, if the magnetic loss originates mainly from the eddy current effect, C_0 will keep a constant over 2−18 GHz. As shown in Figure 3f, in spite of a small fluctuation, the C_0 decreases sharply with an increase of frequency. Thus, the eddy current effect is not a major reason for the magnetic loss of Ni@NG/NC nanosheets.

According to the natural resonance equation $2\pi f_r = \gamma H_a$, where f_r is the natural resonance frequency, γ is the gyromagnetic ratio, and H_a is the anisotropy energy, f_r for bulk nickel should be around several tens of megahertz. However, when the size of nickel is decreased to the nanometer scale, the f_r will shift toward the high-frequency region. For example, f_r was shifted to 5.5 GHz for Ni/C nanocapsules[47] with a diameter of 25−30 nm, while it was located at 16.6 GHz for Ni/ZnO nanocapsules[6] with a diameter of 5−25 nm. In our Ni@NG/NC nanosheets, the natural resonance frequency is observed to be around 9.0 GHz, as shown in Figure 3d. Therefore, the natural resonance contributes to the magnetic loss of the Ni@NG/NC nanosheets. In addition, a weak resonance peak centered at 16.5 GHz can be observed in the Figure 3d. In general, the exchange resonance occurs at a higher frequency than the natural resonance.[5,14] Therefore, we think that the resonance peak at 16.5 GHz is relevant to the exchange resonance. However, the intensity of the exchange resonance peak is greatly weaker than that of the natural resonance peak, and thus, the contribution of the exchange resonance to the magnetic loss of the Ni@NG/NC nanosheets is negligible in comparison to the natural resonance.

3.4. Effect of Ni Content on the EMW Absorption Properties of Ni@NG/NC Nanosheets. In order to study the effect of the Ni content in the nanosheets on the EMW absorption property, two additional samples were prepared by adjusting the molar ratio of urea to nickel acetylacetonate precursors (r). The sample discussed above was synthesized as r = 6:1, and is denoted as Ni@NG/NC-6:1 hereafter. As r values were tuned to be 3:1 and 9:1, two corresponding samples were denoted as Ni@NG/NC-3:1 and Ni@NG/NC-

DOI: 10.1021/acsami.7b15559
ACS Appl. Mater. Interfaces 2018, 10, 1399−1407

9:1, respectively. TG analyses suggest that the Ni contents in Ni@NG/NC-3:1 and Ni@NG/NC-9:1 are 68.0 and 47.9 wt %, respectively, as shown in Figure S10 (Supporting Information). Ni@NG/NC-3:1 and Ni@NG/NC-9:1 show sheetlike morphologies, similar to that Ni@NG/NC-6:1 (Figure 4, parts a and c). However, the densities of Ni NPs in Ni@NG/NC-3:1 and Ni@NG/NC-9:1 are larger and smaller than that in Ni@NG/NC-6:1, respectively (Figure 4, parts a and c). Furthermore, some nanosheets without Ni NPs are found in the Ni@NG/NC-9:1 (Figure S11, Supporting Information). The results above demonstrate that the r value is a crucial factor to obtain ideal Ni@NG/NC nanosheets with uniform distribution of Ni NPs. HRTEM images (Figure 4, parts b and d) reveal that the Ni NPs in Ni@NG/NC-3:1 and Ni@NG/NC-9:1 are encapsulated in few-layer N-doped graphene, similar to those in Ni@NG/NC-6:1. The well-resolved lattice fringes are observed in the Ni region, suggesting the crystal nature of Ni NPs in Ni@NG/NC-3:1 and Ni@NG/NC-9:1. The labeled lattice distances are 0.20 nm, corresponding to (111) planes of Ni NPs.

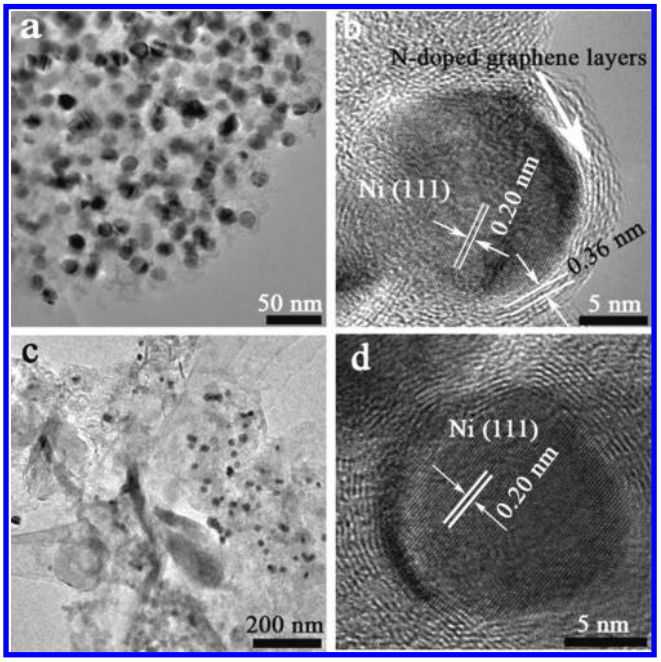

Figure 4. (a and b) TEM and HRTEM images of Ni@NG/NC-3:1 and (c and d) TEM and HRTEM images of Ni@NG/NC-9:1.

The EMW absorption properties of the paraffin composites containing 20 wt % of the Ni@NG/NC-3:1 and Ni@NG/NC-9:1 were also investigated. Figure 5 shows the R_L–f curves of the Ni@NG/NC-3:1 and Ni@NG/NC-9:1 at various thicknesses. Compared to Ni@NG/NC-6:1, the Ni@NG/NC-3:1 exhibits enhanced EMW absorption properties (Figure 5a). For example, the EABs for the Ni@NG/NC-3:1 are 5.7, 8.5, 5.6, 5.3, 5.1, and 4.7 GHz at the thicknesses of 2.5, 3.0, 4.0, 4.5, and 5.0 mm, respectively, significantly larger than the EABs for the Ni@NG/NC-6:1 at the corresponding thickness (Table S2, Supporting Information). Furthermore, the $R_{L,min}$ values for the Ni@NG/NC-3:1 at the thickness ranging from 2.5 to 5.0 mm are less than those for the Ni@NG/NC-6:1 (Table S1, Supporting Information). By comparing the parameters data and the loss tangents between the two samples (Figures S12 and S13, Supporting Information), we find that the enhanced EMW absorption properties of the Ni@NG/NC-3:1 can be explained by its larger dielectric and magnetic losses. On the other hand, the Ni@NG/NC-9:1 exhibits inferior EMW absorption property to the Ni@NG/NC-3:1 including smaller EAB and larger $R_{L,min}$ values. As shown in Figure 5b and Table S2 (Supporting Information), the $R_{L,min}$ values of the Ni@NG/NC-9:1 are less than −10.5 dB. As shown in Figures S12 and S14 (Supporting Information), the inferior EMW absorption property of the Ni@NG/NC-9:1 can be attributed to its smaller dielectric and magnetic losses in comparison to those of the Ni@NG/NC-6:1. In terms of the results above, it can be concluded that the EMW absorption property of the Ni@NG/NC nanosheets can be tuned by the Ni content.

3.5. Effect of N Content on the EMW Absorption Properties of Ni@NG/NC Nanosheets. The N content in our Ni@NG/NC nanosheets can be tuned by the carbonization temperature. We prepared an additional three samples under the same experimental conditions except that the carbonization temperature was changed. The three samples obtained at 800, 1000, and 1100 °C were denoted as Ni@NG/NC-800, Ni@NG/NC-1000, and Ni@NG/NC-1100, respectively. XRD patterns show that the samples contain metallic Ni (Figure S15, Supporting Information). TG analyses indicate that the Ni contents in the Ni@NG/NC-800, Ni@NG/NC-1000, and Ni@NG/NC-1100 about are 51.3, 56.6, and 56.3 wt %,

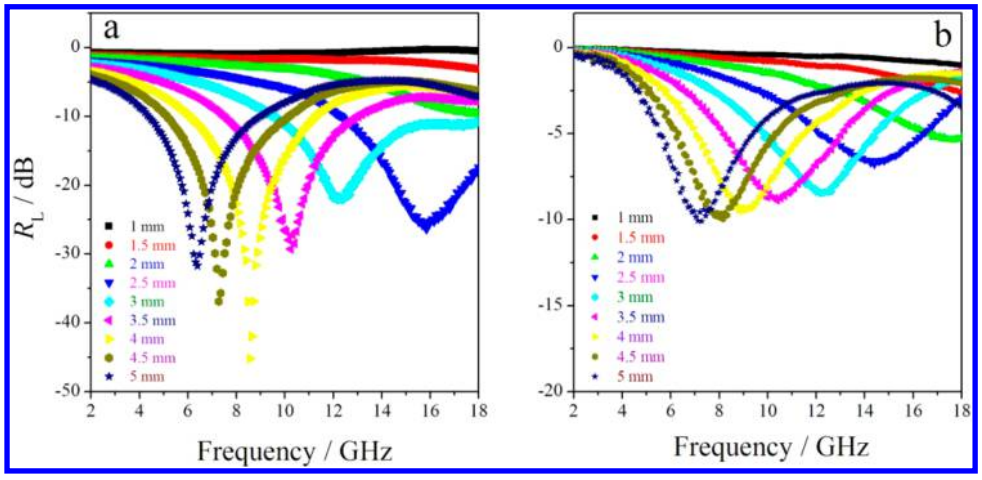

Figure 5. R_L–f curves for Ni@NG/NC-3:1 (a) and Ni@NG/NC-9:1 (b).

DOI: 10.1021/acsami.7b15559
ACS Appl. Mater. Interfaces 2018, 10, 1399−1407

respectively, close to that of Ni@NG/NC-6:1 (Figure S16, Supporting Information). The diameters of Ni NPs in the Ni@NG/NC-800, Ni@NG/NC-1000, and Ni@NG/NC-1100 are around 22, 23, and 26 nm, as shown in Figure S17a–c (Supporting Information). The Ni NPs in the three samples are also coated by N-doped few-layer graphene (Figure S17d–f, Supporting Information). The labeled lattice distances are 0.20 nm, corresponding to (111) planes of Ni NPs, as shown in the insets in Figure S17d–f (Supporting Information). The N contents in the Ni@NG/NC-800, Ni@NG/NC-1000, and Ni@NG/NC-1100 determined by XPS spectra are about 3.7, 0.3, and 0.1 atom % (Figures S18–S20, Supporting Information). The N content is remarkably decreased with the increase of the carbonization temperature, consistent with the previous report.[49] According to the measurements above, Ni@NG/NC-800, Ni@NG/NC-1000, and Ni@NG/NC-1100 have similar morphologies, sizes of Ni NPs, and the Ni contents to those of Ni@NG/NC-6:1; however, the N contents in the three samples are greatly different from that of Ni@NG/NC-6:1, providing us a chance to study the effect of N content on the EMW absorption properties of Ni@NG/NC nanosheets.

The EMW absorption properties of the paraffin composites containing 20 wt % of the Ni@NG/NC-800, Ni@NG/NC-1000, and Ni@NG/NC-1100 were also measured. Figure S21 (Supporting Information) displays the R_L–f curves of the Ni@NG/NC-800, Ni@NG/NC-1000, and Ni@NG/NC-1100 at various thicknesses. Compared to Ni@NG/NC-6:1, the Ni@NG/NC-800 exhibits enhanced EMW absorption properties (Figure S21a, Supporting Information) at smaller thicknesses. For example, the EABs for the Ni@NG/NC-800 are 7.1 and 5.2 GHz at the thicknesses of 2.5 and 3.0 mm, while they are 5.5 and 4.7 GHz for the Ni@NG/NC-6:1, respectively (Table S3, Supporting Information). In view of the practical application, it is desirable that the absorbers can attenuate effectively EMW energy at a thickness as small as possible. In contrast, the Ni@NG/NC-1000 and Ni@NG/NC-1100 show inferior EMW absorption properties at all tested thicknesses including low EAB value and the $R_{L,min}$ values, as shown in Figure S21, parts b and c (Supporting Information) and Table S3 (Supporting Information). Their inferior EMW absorption properties can be attributed to their lower dielectric losses, as shown in Figures S22 and S23 (Supporting Information). Thus, the N elements in our Ni@NG/NC nanosheets play a positive effect on the EMW absorption property. The reason for the positive of the N doping may be related to the different electronegativity between C and N atoms, resulting in partial positive and negative charges in the adjacent C and N species, respectively. Such adjacent C and N species can serve as polarization centers, which can enhance the dielectric loss of the nitrogen-doped carbonaceous materials upon electromagnetic wave irradiation.

4. CONCLUSIONS

In summary, nickel NPs with a diameter of about 20 nm encapsulated six-layers nitrogen-doped graphene supported by nitrogen-doped graphite sheets can be fabricated by a facile method. Two processes, carbonization at a high temperature and subsequent treatment in hot acid solution, were involved in the preparation of the heteronanostructures, and mass-production was achieved easily. The fabricated heteronanostructures exhibit excellent EMW absorption property including strong absorption capability and lightweight feature, comparable to most absorbing materials recently reported. Typically, the EAB is up to 8.5 GHz at the thicknesses of 3.0 mm for the heteronanostructures with the optimized Ni content as the addition amount the heteronanostructures is only 20 wt %. Furthermore, due to the nitrogen-doped graphene shell the Ni NPs have robust stability against strong acidic solution and strong antioxidation upon air exposure. Therefore, the heteronanostructures are very promising for the practical applications in the EM absorption field.

■ ASSOCIATED CONTENT

Supporting Information

The Supporting Information is available free of charge on the ACS Publications website at DOI: 10.1021/acsami.7b15559.

SEM and TEM images, SAED pattern, nitrogen adsorption/desorption isotherms and pore size distribution, XRD patterns, TG curves, relative permittivity and permeability data, loss tangents, XPS spectra, R_L–f curves, and comparisons of EM wave absorption properties (PDF)

■ AUTHOR INFORMATION

Corresponding Authors

*E-mail: zhuchunling@hrbeu.edu.cn.

*E-mail: chenyujin@hrbeu.edu.cn.

ORCID

Yujin Chen: 0000-0002-6794-2276

Notes

The authors declare no competing financial interest.

■ ACKNOWLEDGMENTS

This work is supported by the National Natural Science Foundation of China (Grant No. 51572051), the Natural Science Foundation of Heilongjiang Province (E2016023), the Fundamental Research Funds for the Central Universities (GK2110260179 and GK2110260188), the 111 project (B13015) of Ministry of Education of China to the Harbin Engineering University, the Ph.D. Student Research and Innovation Fund of the Fundamental Research Funds (HEUGIP201714) for the Central Universities, and also the Open Project Program (PEBM201508) of the Key Laboratory for Photonic and Electric Bandgap Materials, Ministry of Education, Harbin Normal University, China.

■ REFERENCES

(1) Bregar, V. Advantages of Ferromagnetic Nanoparticle Composites in Microwave Absorbers. *IEEE Trans. Magn.* **2004**, *40*, 1679–1684.

(2) Lee, C. C.; Chen, D. H. Ag Nanoshell-induced Dual-frequency Electromagnetic Wave Absorption of Ni Nanoparticles. *Appl. Phys. Lett.* **2007**, *90*, 193102.

(3) Lee, C. C.; Cheng, Y. Y.; Chang, H. Y.; Chen, D. H. Synthesis and Electromagnetic Wave Absorption Property of Ni–Ag Alloy Nanoparticles. *J. Alloys Compd.* **2009**, *480*, 674–680.

(4) Wang, H.; Guo, H.; Dai, Y. Y.; Geng, D. Y.; Han, Z.; Li, D.; Yang, T.; Ma, S.; Liu, W.; Zhang, Z. Optimal Electromagnetic-Wave Absorption by Enhanced Dipole Polarization in Ni/C Nanocapsules. *Appl. Phys. Lett.* **2012**, *101*, 083116.

(5) Wen, F.; Yi, H. B.; Qiao, L.; Zheng, H.; Zhou, D.; Li, F. S. Analyses on Double Resonance Behavior in Microwave Magnetic Permeability of Multiwalled Carbon Nanotube Composites Containing Ni Catalyst. *Appl. Phys. Lett.* **2008**, *92*, 042507.

(6) Liu, X. G.; Jiang, J. J.; Geng, D. Y.; Li, B. Q.; Han, Z.; Liu, W.; Zhang, Z. D. Dual Nonlinear Dielectric Resonance and Strong Natural

Resonance in Ni/ZnO Nanocapsules. *Appl. Phys. Lett.* **2009**, *94*, 053119.
(7) Zhao, B.; Shao, G.; Fan, B. B.; Zhao, W. Y.; Zhang, R. Investigation of The Electromagnetic Absorption Properties of Ni@TiO_2 and Ni@SiO_2Composite Microspheres with Core-shell Structure. *Phys. Chem. Chem. Phys.* **2015**, *17*, 2531−2539.
(8) Li, N.; Cao, M.; Hu, C. A Simple Approach to Spherical Nickel-Carbon Monoliths As Light-Weight Microwave Absorbers. *J. Mater. Chem.* **2012**, *22*, 18426−18432.
(9) An, Z. Q.; Zhang, J. Q. Facile Large Scale Preparation and Electromagnetic Properties of Silica−Nickel−Carbon Composite Shelly Hollow Microspheres. *Dalton. Trans.* **2016**, *45*, 2881−2887.
(10) Zhao, B.; Guo, X.; Zhao, W.; Deng, J. H.; Shao, G.; Fan, B. B.; Bai, Z. Y.; Zhang, R. Yolk-Shell Ni@SnO_2 Composites with a Designable Interspace to Improve Electromagnetic Wave Absorption Properties. *ACS Appl. Mater. Interfaces* **2016**, *8*, 28917−28925.
(11) Zhao, B.; Shao, G.; Fan, B.; Zhao, W. Y.; Xie, Y. J.; Zhang, R. ZnS Nanowall Coated Ni Composites: Facile Preparation and Enhanced Electromagnetic Wave Absorption. *RSC Adv.* **2014**, *4*, 61219−61225.
(12) Zhao, B.; Fan, B.; Shao, G.; Zhao, W. Y.; Zhang, R. Facile Synthesis of Novel Heterostructure Based on SnO_2Nanorods Grown on Submicron Ni Walnut with Tunable Electromagnetic Wave Absorption Capabilities. *ACS Appl. Mater. Interfaces* **2015**, *7*, 18815−18823.
(13) Tong, G. X.; Liu, F. T.; Wu, W. H.; Du, F. F.; Guan, J. G. Rambutan-like Ni/MWCNT Heterostructures: Easy Synthesis, Formation Mechanism, and Controlled Static Magnetic and Microwave Electromagnetic Characteristics. *J. Mater. Chem. A* **2014**, *2*, 7373−7382.
(14) Wang, G. Z.; Peng, X. G.; Yu, L.; Wan, G. P.; Lin, S. W.; Qin, Y. Enhanced Microwave Absorption of ZnO Coated with Ni Nanoparticles Produced by Atomic Layer Deposition. *J. Mater. Chem. A* **2015**, *3*, 2734−2740.
(15) Che, R. C.; Peng, L. M.; Duan, X. F.; Chen, Q.; Liang, X. L. Microwave Absorption Enhancement and Complex Permittivity and Permeability of Fe Encapsulated within Carbon Nanotubes. *Adv. Mater.* **2004**, *16*, 401−405.
(16) Qiu, S.; Lyu, H. L.; Liu, J. R.; Liu, Y. Z.; Wu, N. N.; Liu, W. Facile Synthesis of Porous Nickel/Carbon Composite Microspheres with Enhanced Electromagnetic Wave Absorption by Magnetic and Dielectric Losses. *ACS Appl. Mater. Interfaces* **2016**, *8*, 20258−20266.
(17) Ding, D.; Wang, Y.; Li, X. D.; Qiang, R.; Xu, P.; Chu, W. L.; Han, X. J.; Du, Y. C. Rational Design of Core-shell Co@C Microspheres for High-performance Microwave Absorption. *Carbon* **2017**, *111*, 722−732.
(18) Liu, T.; Xie, X. B.; Pang, Y.; Kobayashi, S. Co/C Nanoparticles with Low Graphitization Degree: a High Performance Microwave-Absorbing Material. *J. Mater. Chem. C* **2016**, *4*, 1727−1735.
(19) Singh, V. K.; Shukla, A.; Patra, M. K.; Saini, L.; Jani, R. K.; Vadera, S. R.; Kumar, N. Microwave Absorbing Properties of a Thermally Reduced Graphene Oxide/Nitrile Butadiene Rubber Composite. *Carbon* **2012**, *50*, 2202−2208.
(20) Chen, Y. J.; Wang, Q. S.; Zhu, C. L.; Gao, P.; Ouyang, Q. Y.; Wang, T. S.; Ma, Y.; Sun, C. W. Graphene/Porous Cobalt Nanocomposite and Its Noticeable Electrochemical Hydrogen Storage Ability at Room Temperature. *J. Mater. Chem.* **2012**, *22*, 5924−5927.
(21) Song, C. Q.; Yin, X. W.; Han, M. K.; Li, X. L.; Hou, Z. X.; Zhang, L. T.; Cheng, L. F. Three-Dimensional Reduced Graphene Oxide Foam Modified with ZnO Nanowires for Enhanced Microwave Absorption Properties. *Carbon* **2017**, *116*, 50−58.
(22) Feng, W.; Wang, Y. M.; Chen, J. C.; Wang, L.; Guo, L. X.; Ouyang, J. H.; Jia, D. C.; Zhou, Y. Reduced Graphene Oxide Decorated with In-situ Growing ZnO Nanocrystals: Facile Synthesis and Enhanced Microwave Absorption Properties. *Carbon* **2016**, *108*, 52−60.
(23) Wang, T. S.; Liu, Z. L.; Lu, M. M.; Wen, V.; Ouyang, Q. Y.; Chen, Y. J.; Zhu, C. L.; Gao, P.; Li, C. Y.; Cao, M. S.; Qi, L. H. Graphene−Fe_3O_4Nanohybrids: Synthesis and Excellent Electromagnetic Absorption Properties. *J. Appl. Phys.* **2013**, *113*, 024314.
(24) Ren, Y. L.; Wu, H. Y.; Lu, M. M.; Chen, Y. J.; Zhu, C. L.; Gao, P.; Cao, M. S.; Li, C. Y.; Ouyang, Q. Y. Quaternary Nanocomposites Consisting of Graphene, Fe_3O_4@Fe Core@Shell, and ZnO Nanoparticles: Synthesis and Excellent Electromagnetic Absorption Properties. *ACS Appl. Mater. Interfaces* **2012**, *4*, 6436−6442.
(25) Cao, Y.; Su, Q.; Che, R.; Du, G.; Xu, B. One-step Chemical Vapor Synthesis of Ni/Graphene Nanocomposites with Excellent Electromagnetic and Electrocatalytic Properties. *Synth. Met.* **2012**, *162*, 968−973.
(26) Ding, Y.; Liao, Q. L.; Liu, S.; Guo, H. J.; Sun, Y. H.; Zhang, G. J.; Zhang, Y. Reduced Graphene Oxide Functionalized with Cobalt Ferrite Nanocomposites for Enhanced Efficient and Light weight Electromagnetic Wave Absorption. *Sci. Rep.* **2016**, *6*, 32381.
(27) Liu, W. W.; Li, H.; Zeng, Q. P.; Duan, H. N.; Guo, Y. P.; Liu, X. F.; Sun, C. Y.; Liu, H. Z. Fabrication of Ultralight Three-Dimensional Graphene Networks with Strong Electromagnetic Wave Absorption Properties. *J. Mater. Chem. A* **2015**, *3*, 3739−3747.
(28) Ren, Y. L.; Zhu, C. L.; Zhang, S.; Li, C. Y.; Chen, Y. J.; Gao, P.; Yang, P. P.; Ouyang, Q. Y. Three-dimensional SiO_2@Fe_3O_4Core/Shell Nanorod Array/Graphene Architecture: Synthesis and Electromagnetic Absorption Property. *Nanoscale* **2013**, *5*, 12296−12303.
(29) Han, M. K.; Yin, X. W.; Kong, L.; Li, M.; Duan, W. Y.; Zhang, L. T.; Cheng, L. F. Graphene-wrapped ZnO Hollow Spheres with Enhanced Electromagnetic Wave Absorption Properties. *J. Mater. Chem. A* **2014**, *2*, 16403−16409.
(30) Liu, T. H.; Lee, S. C.; Pao, C. W.; Chang, C. C. Anomalous Thermal Transport Along the Grain Boundaries of Bicrystalline Graphene Nanoribbons from Atomistic Simulations. *Carbon* **2014**, *73*, 432−442.
(31) Sun, D. P.; Zou, Q.; Wang, Y. P.; Wang, Y. J.; Jiang, W.; Li, F. S. Controllable Synthesis of Porous Fe_3O_4@ZnO Sphere Decorated Graphene for Extraordinary Electromagnetic Wave Absorption. *Nanoscale* **2014**, *6*, 6557−6562.
(32) Pan, G. H.; Zhu, J.; Ma, S. L.; Sun, G. B.; Yang, X. J. Enhancing the Electromagnetic Performance of Co Through the Phase-Controlled Synthesis of Hexagonal and Cubic Co Nanocrystals Grown on Graphene. *ACS Appl. Mater. Interfaces* **2013**, *5*, 12716−12724.
(33) Fu, M.; Jiao, Q. Z.; Zhao, Y.; Li, H. S. Vapor Diffusion Synthesis of $CoFe_2O_4$ Hollow Sphere/Graphene Composites as Absorbing Materials. *J. Mater. Chem. A* **2014**, *2*, 735−744.
(34) Qu, B.; Zhu, C. L.; Li, C. Y.; Zhang, X. T.; Chen, Y. J. Coupling hollow Fe_3O_4-Fe Nanoparticles with Graphene Sheets for High-performance Electromagnetic Wave Absorbing Material. *ACS Appl. Mater. Interfaces* **2016**, *8*, 3730−3735.
(35) Feng, J. T.; Hou, Y. H.; Wang, Y. C.; Li, L. C. Synthesis of Hierarchical $ZnFe_2O_4$@SiO_2@RGO Core−Shell Microspheres for Enhanced Electromagnetic Wave Absorption. *ACS Appl. Mater. Interfaces* **2017**, *9*, 14103−14111.
(36) Kong, L.; Yin, X. W.; Zhang, Y. J.; Yuan, X. Y.; Li, Q.; Ye, F.; Cheng, L. F.; Zhang, L. T. Electromagnetic Wave Absorption Properties of Reduced Graphene Oxide Modified by Maghemite Colloidal Nanoparticle Clusters. *J. Phys. Chem. C* **2013**, *117*, 19701−19711.
(37) Bai, X.; Zhai, Y. H.; Zhang, Y. Green Approach to Prepare Graphene-based Composites with High Microwave Absorption Capacity. *J. Phys. Chem. C* **2011**, *115*, 11673−11677.
(38) Fu, M.; Jiao, Q. Z.; Zhao, Y. Preparation of $NiFe_2O_4$ Nanorod−Graphene Composites Via an Ionic Liquid Assisted One-step Hydrothermal Approach and Their Microwave Absorbing Properties. *J. Mater. Chem. A* **2013**, *1*, 5577−5586.
(39) Qi, X. S.; Hu, Q.; Cai, H. B.; Xie, R.; Bai, Z. C.; Jiang, Y.; Qin, S. J.; Zhong, W.; Du, Y. W. Heteronanostructured Co@carbon Nanotubes-graphene Ternary Hybrids: Synthesis, Electromagnetic and Excellent Microwave Absorption Properties. *Sci. Rep.* **2016**, *6*, 37972.

DOI: 10.1021/acsami.7b15559
ACS Appl. Mater. Interfaces 2018, 10, 1399−1407

(40) Kenney, M. J.; Gong, M.; Li, Y. G.; Wu, J. Z.; Feng, J.; Lanza, M.; Dai, H. J. High-Performance Silicon Photoanodes Passivated with Ultrathin Nickel Films for Water Oxidation. *Science* **2013**, *342*, 836−840.
(41) Li, X. L.; Wang, H. L.; Robinson, J. T.; Sanchez, H.; Diankov, G.; Dai, H. J. Simultaneous Nitrogen Doping and Reduction of Graphene Oxide. *J. Am. Chem. Soc.* **2009**, *131*, 15939−15944.
(42) Deng, J.; Ren, P. J.; Deng, D. H.; Yu, L.; Yang, F.; Bao, X. H. Highly Active and Durable Non-Precious-Metal Catalysts Encapsulated in Carbon Nanotubes for Hydrogen Evolution Reaction. *Energy Environ. Sci.* **2014**, *7*, 1919−1923.
(43) Sheng, Z. H.; Shao, L.; Chen, J. J.; Bao, W. J.; Wang, F. B.; Xia, X. H. Catalyst-Free Synthesis of Nitrogen Doped Graphene via Thermal Annealing Graphite Oxide with Melamine and Its Excellent Electrocatalysis. *ACS Nano* **2011**, *5*, 4350−4358.
(44) Naito, Y.; Suetake, K. Application of Ferrite to Electromagnetic Wave Absorber and Its Characteristics. *IEEE Trans. Microwave Theory Tech.* **1971**, *19*, 65−72.
(45) Frenkel, J.; Doefman, J. Spontaneous and Induced Magnetisation in Ferromagnetic Bodies. *Nature* **1930**, *126*, 274−275.
(46) Wu, M. Z.; Zhang, Y. D.; Hui, S.; Xiao, T. D.; Ge, S. H.; Hines, W. A.; Budnick, J. I.; Taylor, G. W. *Appl. Phys. Lett.* **2002**, *80*, 4404.
(47) Zhang, X. F.; Dong, X. L.; Huang, H.; Liu, Y. Y.; Wang, W. N.; Zhu, X. G.; Lv, B.; Lei, J. P.; Lee, C. G. Microwave Absorption Properties of the Carbon-coated Nickel Nanocapsules. *Appl. Phys. Lett.* **2006**, *89*, 053115.
(48) Yu, X. B.; Qu, B.; Zhao, Y.; Li, C. Y.; Chen, Y. J.; Sun, C. W.; Gao, P.; Zhu, C. L. Growth of Hollow Transition Metal (Fe, Co, Ni) Oxide Nanoparticles on Graphene Sheets through Kirkendall Effect as Anodes for High-Performance Lithium-Ion Batteries. *Chem. - Eur. J.* **2016**, *22*, 1638−1645.
(49) Zhang, K.; Zhao, Y.; Fu, D. Y.; Chen, Y. J. Molybdenum Carbide Nanocrystals Embedded N-doped Carbon Nanotubes as Electrocatalysts for Hydrogen Generation. *J. Mater. Chem. A* **2015**, *3*, 5783−5788.

DOI: 10.1021/acsami.7b15559
ACS Appl. Mater. Interfaces 2018, 10, 1399−1407